JOURNAL OF Materials CHEMISTRY

Nanoporous silica particles prepared by chemical reactivity of ORMOSILs

Pierre M. Chevalier* and Duan Li Ou

Dow Corning Ltd., Cardiff Road, Barry, South Glamorgan, UK CF63 2YL.
E-mail: p.chevalier@dowcorning.com

Received 5th April 2002, Accepted 27th June 2002
First published as an Advance Article on the web 27th August 2002

Hybrid organic–inorganic particles containing labile organic templates have been prepared by either controlled sol–gel processing or co-condensation of colloidal silica particles with organosilicon precursors. Chemical removal of the templating organic spacer led to monomodal, porous microstructured silica particles exhibiting up to 50% porosity. Particle size and distribution, and porosity varied depending upon the process and the chemistry used to remove the porogen organic groups.

Introduction

Dense silica nanoparticles have received considerable attention since monodisperse colloidal silica spheres, obtained from ammoniacal TEOS (tetraethylorthosilicate, $Si(OC_2H_5)_4$) solution, were reported in the late 1960's by Stöber *et al.*[1] The particles prepared by acid or base hydrolysis-condensation of TEOS,[1–10] have a non-porous core and a relatively low surface area directly related to the size of the particles. These particles, more often having a high monodispersity with controlled particle size, a well-defined morphology, and a surface with silanol groups by which they could be functionalised, are used for a variety of commercial applications including colorants, fillers and pigments.

Similarly, the engineering of porosity in common materials such as silica has been emerging as a new area of great technological and scientific interest;[11–16] activity has dramatically increased since the development of the MCM-type of materials.[12] Materials with tailor-made pore sizes and shapes are particularly important in applications where molecular recognition is needed, such as shape-selective catalysis, molecular sieving, chemical sensing and selective adsorption.[17,18] Thus, mesoporous materials with well-defined pore sizes ranging from 2 to 50 nm have been synthesised successfully *via* self-assembly of surfactants and inorganic metal oxides.[12,19]

However, it recently became desirable to be able to synthesize porous silica nanoparticles, having both a narrow monodispersity and a well-defined pore size and connectivity, for a wider range of applications: catalysis, separation, chromatography, controlled release, low relative permittivity fillers, custom-designed pigments, and optical hosts.[19–23]

The preparation of nanostructured silica particles is usually done by a combination of former approaches involving the synthesis of silica spheres from catalysed hydrolysis–condensation of alkoxysilane combined with the use of templating agents, *e.g.*, surfactant micelles,[24,25] complexing salts,[26] polystyrene beads[24] or polymer latex spheres;[22,27,28] templates being removed by calcination at a temperature ranging from 400 to 800 °C. Porous micro- to nano-structured silica particles, with surface areas below 450 $m^2\ g^{-1}$, were then prepared assisted by various constraining processes: *e.g.*, rapid aerosol,[24] ultrasonic spray,[29] water-in-oil emulsion,[30] emulsion-templating process,[31] and other "spinodal decomposition-type" processes.[26]

This paper reports the continuing investigation of hybrid organic–inorganic materials containing a removable organic template leading, after chemical treatment, to porous silica with narrow pore size distribution.[32] We previously reported that hybrid silsesquioxane gels containing acetylenic bridging units led to silica upon mild NH_4F catalysed hydrolysis. In the case of a rigid bridging unit, the resulting material obtained was a mesoporous silica, having a high surface area up to 800 $m^2\ g^{-1}$, and a very narrow pore-size distribution.

We wish to report here two routes for the preparation of porous silica particles through the temporary incorporation of chemically labile organic templating fragments. ORMOSIL (organically modified silicate) particles are prepared in a first step by either a "controlled" hydrolysis–condensation process or by co-condensation of colloidal silica nanoparticles with organosilicon precursors leading, after chemical removal of the templating organic spacer, to porous monomodal silica particles.

Results and discussion

The first multi-step route towards the preparation of nanoporous silica particles involved the formation of ORMOSIL particles through "controlled" hydrolysis–condensation of the bridged organosilicon precursor 1,4-bis(trimethoxysilylethynyl)benzene (Scheme 1).

The colloidal particles were quenched at the sol stage using *N,O*-bis(trimethylsilyl) carbamate (BSC) capping agent leading to hybrid particles **H**. Then the organic spacer was chemically removed by $Si–C_{sp}$ bond cleavage leading to particles **A**, and the particles further calcined at 600 °C under air, yielding carbon-free porous silica particles **B**.

Two sets of hybrid particles $\mathbf{H_1}$ and $\mathbf{H_2}$ were then both prepared by capping the hybrid sol. Particles $\mathbf{H_1}$ were obtained by carrying out the reaction at room temperature leading to a polydispersion of particles through the exothermic formation of a soft gel. Particles $\mathbf{H_2}$ were prepared by a more careful quenching reaction of the sol in dilute conditions and at lower temperature from −5 °C to room temperature. The characterisation of the resulting hybrid particles $\mathbf{H_1}$ and $\mathbf{H_2}$ by ^{13}C, ^{29}Si CP MAS NMR and FTIR spectroscopies confirmed that the organic structure was maintained during the hydrolysis–condensation and quenching reaction, and that no, or minor, $Si–C_{sp}$ bond cleavage had occurred during those reaction steps leading to hybrid organic–inorganic particles. Indeed the ^{13}C NMR spectra showed the expected resonances associated with the bridging organic fragment: aromatic carbon atoms at *ca.* 123 and 132 ppm and two acetylenic carbon atoms at *ca.* 90 and 102 ppm, as well as the resonance associated with trimethylsilyl end-groups at *ca.* 1 ppm. Residual uncondensed methoxy

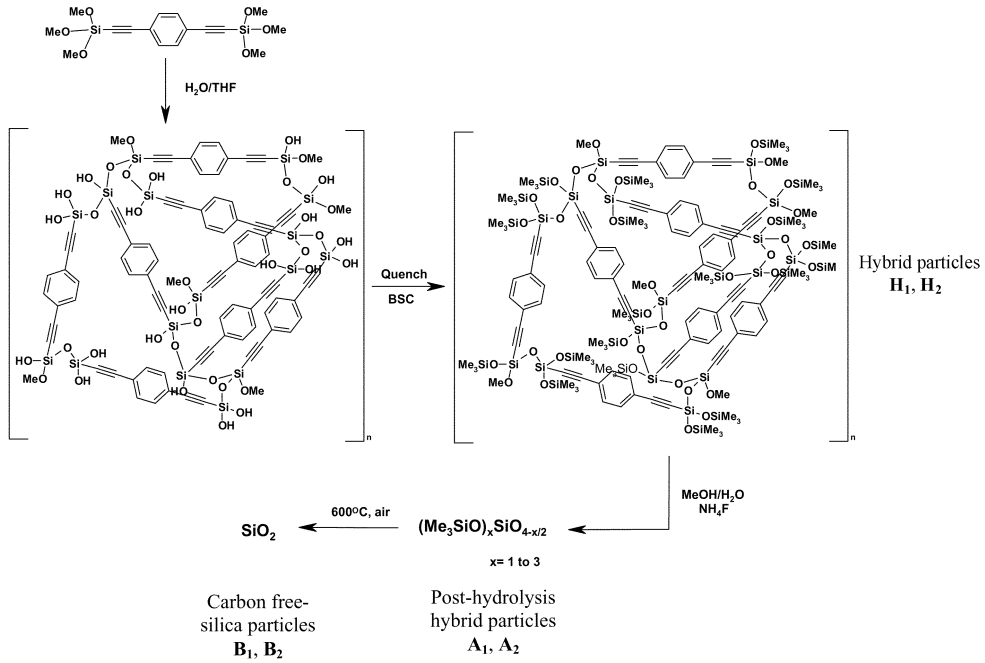

Scheme 1 Organic–inorganic hybrid route to porous silica particles.

Table 1 N_2 BET surface area and porosity properties of hybrids $\mathbf{H_1}$, $\mathbf{H_2}$; post-hydrolysis hybrids $\mathbf{A_1}$, $\mathbf{A_2}$; and carbon-free silica particles $\mathbf{B_1}$ and $\mathbf{B_2}$

Particle	BET Surface area/$m^2\ g^{-1}$	Total pore volume/$cm^3\ g^{-1}$	Micropore surface area/$m^2\ g^{-1}$	Micropore volume/$cm^3\ g^{-1}$	% Porosity
$\mathbf{H_1}$	37	/	/	/	/
$\mathbf{H_2}$	52	/	/	/	/
$\mathbf{A_1}$	257	0.239	229	0.183	26.4
$\mathbf{A_2}$	402	0.326	367	0.256	32.9
$\mathbf{B_1}$	416	0.306	388	0.248	31.5
$\mathbf{B_2}$	339	0.243	318	0.201	26.7

groups in the solid material also showed a resonance at *ca.* 50 ppm. The signals observed by ^{29}Si CP MAS NMR were characteristic of silicon atoms attached to three oxygen atoms and one sp carbon atom: T^1 (CSiOMe)$_2$–(OSi) at −78 ppm being very weak for the hybrid particles $\mathbf{H_1}$ and nonexistent for the hybrid particles $\mathbf{H_2}$, T^2 CSi(OMe)(OSi)$_2$ at −88 ppm and T^3 CSi(OSi)$_3$ at −97 ppm being the major T sub-structure. A very strong resonance is also observed at 12 ppm corresponding to C_3Si(OSi) or M substructure resulting from the Me_3Si capping reaction.

The surface area of these hybrid particles, determined by the BET method using the data from N_2 adsorption isotherms,[33] were low, being 37 and 52 $m^2\ g^{-1}$ respectively for particles $\mathbf{H_1}$ and $\mathbf{H_2}$ (Table 1), and in a similar range to bridged ORMOSILs prepared by the usual sol–gel route.[32]

However, the particle diameter and particle size distributions of $\mathbf{H_1}$ and $\mathbf{H_2}$, determined by a laser particle size analyser, were very different. The particle size distribution of $\mathbf{H_1}$ was very broad and polymodal with particle diameters mainly from 4 to 400 μm, reflecting the inhomogeneity observed during the process due to further aggregation; whereas the controlled quenching of the sol in the case of particle $\mathbf{H_2}$ led to a very narrow monomodal particle size distribution of particle diameters centred at 600 nm (Table 2 and Fig. 1), representing a much simpler process than the Stöber process, and leading to stable and dispersible particles in common organic solvents.

The second step toward the preparation of nanoporous particles, involved the removal of the porogen organic spacer. The cleavage of the Si–C bond in the hybrid silica particles $\mathbf{H_1}$ and $\mathbf{H_2}$ was then achieved upon activation of the silicon atom using a nucleophilic catalyst like NH_4F in an excess of water and methanol, at 65 °C,[32] leading to particles $\mathbf{A_1}$ and $\mathbf{A_2}$ respectively. Characterisation by FTIR and MAS NMR spectroscopies confirmed the Si–C_{sp} cleavage. By ^{29}Si MAS NMR, Q^3 [Si(OH)(OSi)$_3$ or Si(OMe)(OSi)$_3$] and major Q^4 [Si(OSi)$_4$] substructures, at −100 and −110 ppm respectively, were formed during the reaction with retention of the Me_3Si end-groups or M substructures at 12 ppm. Remaining free organic groups were observed in both particles $\mathbf{A_1}$ and $\mathbf{A_2}$, confirming the need for a subsequent thermal treatment at 600 °C under air atmosphere to get carbon-free silica particles, $\mathbf{B_1}$ and $\mathbf{B_2}$.

As a result of the removal of the templating organic group, a large increase in surface area of up to 400 $m^2\ g^{-1}$ was observed for particles $\mathbf{A_1}$ and $\mathbf{A_2}$, after chemical treatment (Table 1), *versus* the low porosity of the starting hybrid particles $\mathbf{H_1}$ and $\mathbf{H_2}$.

The subsequent thermal treatment did not greatly affect the porosity of both materials, as they still had a total pore volume

Table 2 Maximum particle size diameters of hybrid particles $\mathbf{H_1}$ and $\mathbf{H_2}$; post-hydrolysis hybrid particles $\mathbf{A_1}$ and $\mathbf{A_2}$; and carbon-free silica particles $\mathbf{B_1}$ and $\mathbf{B_2}$

	Maximum particle diameter/μm					
Volume (%)	$\mathbf{H_1}$	$\mathbf{H_2}$	$\mathbf{A_1}$	$\mathbf{A_2}$	$\mathbf{B_1}$	$\mathbf{B_2}$
10.00	6.334	0.477	3.247	9.899	1.806	1.613
25.00	31.78	0.538	5.874	15.55	2.765	2.562
50.00	82.00	0.616	12.75	25.11	4.444	4.275
75.00	166.3	0.706	22.88	37.06	6.881	6.827
90.00	214.2	0.791	27.67	47.25	9.544	9.620

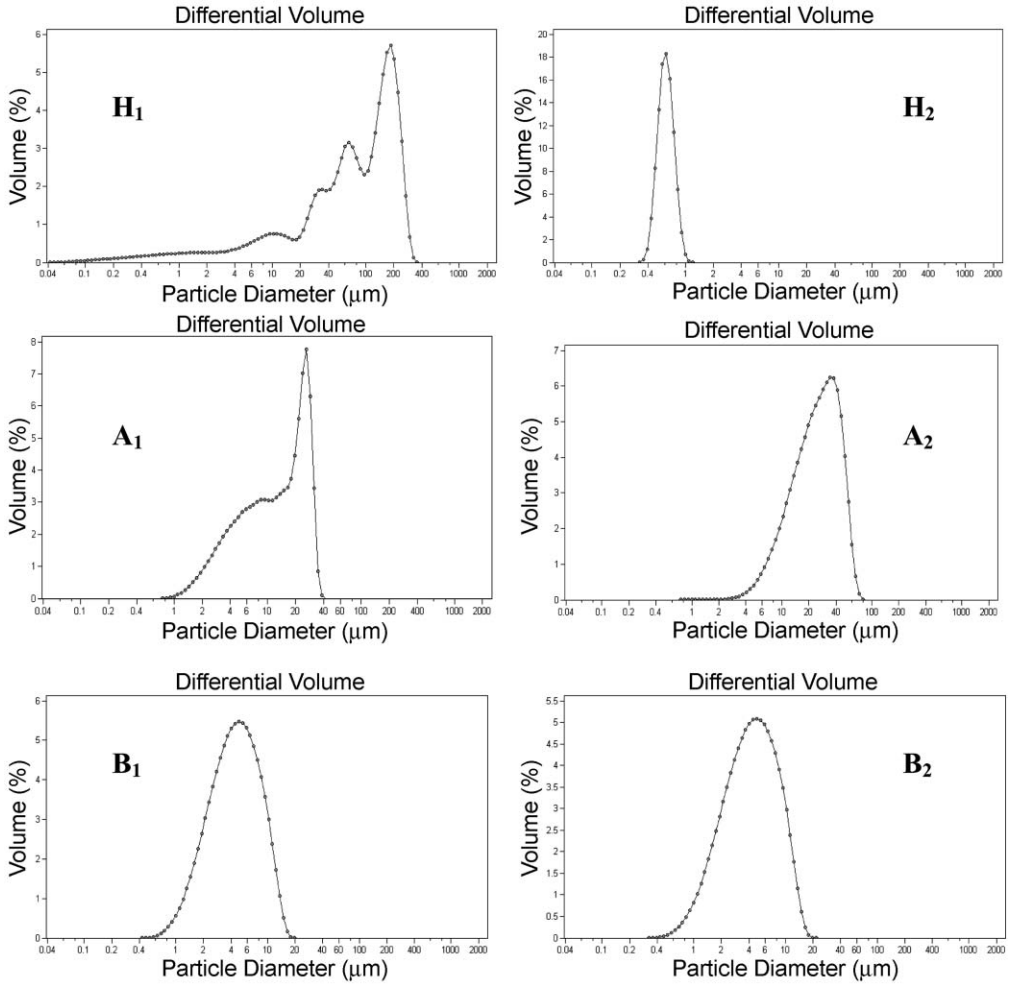

Fig. 1 Particle size distributions of hybrid particles $\mathbf{H_1}$ and $\mathbf{H_2}$; post-hydrolysis hybrid particles $\mathbf{A_1}$ and $\mathbf{A_2}$; and carbon-free silica particles $\mathbf{B_1}$ and $\mathbf{B_2}$.

of from 0.24 to 0.31 $cm^3\ g^{-1}$. The pore size distributions of the carbon-free silica particles $\mathbf{B_1}$ and $\mathbf{B_2}$ after subsequent calcination were also determined by BJH[34] and DFT[35] calculation methods using the data from N_2 sorption isotherms (Fig. 2a and 2b), revealing the formation of largely microporous particles, with some contribution in the mesopore region, being mostly below 50 Å, according to both calculation methods.

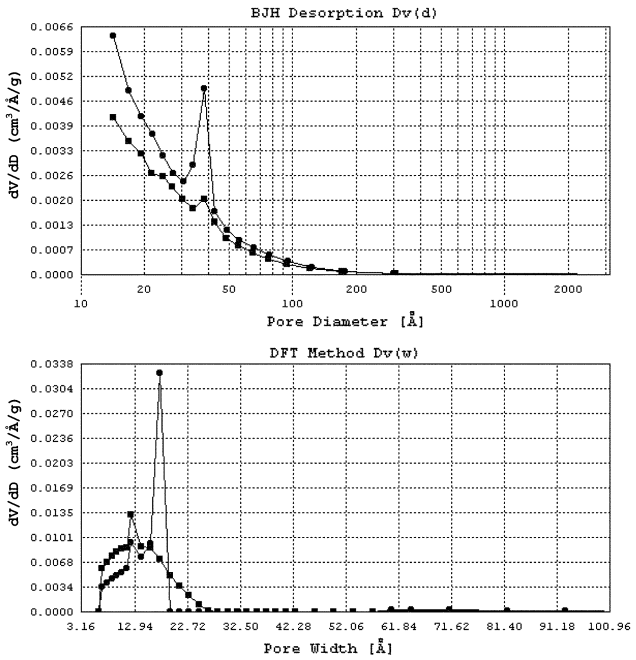

Fig. 2 (a) BJH and (b) DFT pore size distribution of carbon-free silica particles (●: $\mathbf{B_1}$; ■: $\mathbf{B_2}$).

Similarly, the mild removal of the organic spacer strongly modified the size of the particles as shown in Table 2 and Fig. 1. The chemical treatment of particles $\mathbf{H_1}$ aggregated during the capping reaction led to lower particle size $\mathbf{A_1}$, having now a bimodal size distribution, whereas the subsequent thermal treatment, completing the removal of remaining bridged organic spacers as well as of free organics, led to particles $\mathbf{B_1}$ having a monomodal particle size distribution: mainly from 1 to 10 μm and centred at 4 μm. In contrast, the chemical removal of the organic spacer of the sub-micron particles $\mathbf{H_2}$, obtained by a careful quenching of the hydrolysis–condensation of the 1,4-bis(trimethoxysilylethynyl)benzene at the sol stage and at low temperature, led to particles $\mathbf{A_2}$ with a much broader monomodal size distribution of higher particle sizes centred at 25 μm. This phenomenon could easily be explained by the hydrolytic Si–C_{sp} cleavage under nucleophilic catalysis, leading to the removal of the organic spacer with rearrangement of the silicate framework as well as further hydrolysis–condensation of the remaining methoxy groups, both responsible for the particle aggregation. As previously observed, the calcination of particles $\mathbf{A_2}$ at 600 °C under air atmosphere, led to carbon-free particles $\mathbf{B_2}$, still having a monomodal size distribution, but of lower particle sizes centred at 4 μm and almost identical to particles $\mathbf{B_1}$.

This first approach appeared to be interesting as it involved simple steps: preparing nanoporous silica particles through the formation of molecularly defined, organic–inorganic hybrid sub-micron particles by quenching the hydrolysis–condensation

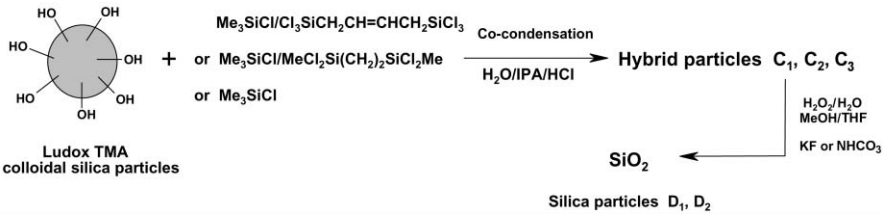

Scheme 2 From dense colloidal silica particles to porous silica particles.

at the sol stage, followed by a mild chemical treatment to remove the porogen organic spacer leading to porous hybrid particles. A subsequent thermal oxidation led to the formation of carbon-free porous particles without any major porosity changes, potentially occurring by rearrangement and pore collapsing, but with overall reduction of the particle sizes to mostly < 10 μm. Nanoporous silica particles, dispersible in common organic solvents and stable under air atmosphere up to 600 °C, were then prepared by this first multi-step route.

However, as we could not prevent particle aggregation through the entire process to obtain porous nanoparticles, we then decided to investigate the formation of hybrid particles by heterocondensation of preformed colloidal silica nanoparticles with bridged organochlorosilanes.

The second multi-step route towards the preparation of porous silica particles also involved the formation of ORMOSIL particles through the co-condensation of pre-formed colloidal silica, being deionised Ludox TMA silica particles of size below 150 nm, and a series of organochlorosilanes. Chlorotrimethylsilane was also used to cap the remaining hydroxy functionalities, thus minimising the particle aggregation (Scheme 2).

1,4-Bis(trichlorosilyl)but-2-ene and chlorotrimethylsilane were pre-hydrolysed under strong acidic conditions, prior to addition of the colloidal silica, leading to particles $\mathbf{C_1}$. An identical procedure was used with 1,2-bis(dichloromethylsilyl)-ethane and chlorotrimethylsilane as well as with chlorotrimethylsilane alone for comparison, leading to particles $\mathbf{C_2}$ and $\mathbf{C_3}$, respectively. These particles were characterised by ^{13}C and ^{29}Si MAS NMR spectroscopy. The ^{13}C MAS NMR spectra showed the expected resonance associated with bridging organic fragments and methyl groups. The ^{29}Si MAS NMR spectra exhibited, depending on the choice of chlorosilane, several sets of signals associated with M (C_3SiO) from 7 to 13 ppm, D (C_2SiO_2) from −9 to −22 ppm, T ($CSiO_3$) from −62 to −70 ppm and Q (SiO_4) substructures from −90 to −120 ppm, arising from the hydrolysis–heterocondensation of organochlorosilanes with the colloidal silica, thus confirming the formation of organic–inorganic particles $\mathbf{C_1}$, $\mathbf{C_2}$ and $\mathbf{C_3}$.

The size and distribution of the particles $\mathbf{C_1}$–$\mathbf{C_3}$ were determined and compared with the pre-formed Ludox TMA silica particles (Table 3, Fig. 3). The average particle diameter, given by the manufacturer as being 22 nm, was re-evaluated giving a narrow particle size distribution, centred at 111 nm; the differences were probably due to concentration changes upon storage and/or change of concentration and pH during the particle analysis in deionised water.

A monomodal particle size distribution was also observed for the hybrid particles $\mathbf{C_1}$–$\mathbf{C_3}$; however, they were much broader than that of the starting colloidal silica, and were centred at higher particle size ranges: 8, 10 and 15 μm, respectively, for $\mathbf{C_1}$, $\mathbf{C_2}$ and $\mathbf{C_3}$. This dramatic increase of the particle size after heterocondensation could be explained by the aggregation of particles during the hydrolysis–co-condensation process, not only promoted by the use of tetra- and hexa-functional bridged organochlorosilanes, but probably also due to the reaction conditions, in terms of pH and concentration, also favouring a colloidal silica particle aggregation, as suggested by the highest particle sizes, $\mathbf{C_3}$, observed when using the monofunctional chlorotrimethylsilane.

The porosity of the particles $\mathbf{C_1}$–$\mathbf{C_3}$ was also determined and compared with that of the pre-formed Ludox TMA silica particles (Table 4, Fig. 4). Ludox TMA particles are dense colloidal silica. The surface area is related to the particle size, being inversely proportional. The surface area of the starting colloidal silica was then estimated to be around 20 $m^2\ g^{-1}$ on the basis of the experimental average particle size of 111 nm determined previously by laser diffraction using the Fraunhofer calculation model.

We observed a slight increase in the surface area after co-condensation of the pre-formed colloidal silica with the organochlorosilane, comparable to the surface area of the hybrid particles $\mathbf{H_1}$ and $\mathbf{H_2}$ described by the first multi-step route. However, the main difference was really the formation of highly porous hybrid particles, up to 50% porosity, having a total pore volume of from 0.64 down to 0.47 $cm^3\ g^{-1}$, from $\mathbf{C_1}$ to $\mathbf{C_3}$, as the average particle size observed earlier increased. The pore size distribution of these particles calculated by the BJH method also revealed the formation of mainly mesoporous particles with some contributions in the micro- and macroporous regions (Fig. 4).

Both the porosity and particle size analysis confirmed the suspected aggregation of the particles during the heterocondensation. The high porosity observed on the particles $\mathbf{C_1}$–$\mathbf{C_3}$ was not only the result of intra-particle porosity, being relatively low and demonstrated by the small microporosity contribution, but was more a consequence of inter-particle porosity, as observed by the main contribution of the pores in the meso- and macro-porous regions (Fig. 4). The particle size was lower for $\mathbf{C_1}$ than for $\mathbf{C_2}$; it was also lower than for $\mathbf{C_3}$, due to the increasing extent of the aggregation phenomenon. Similarly, the mesoporosity, as a result of the particle aggregation, increased for the hybrid particles $\mathbf{C_1}$ to $\mathbf{C_3}$ (Fig. 3 and 4).

Table 3 Maximum particle size diameters of Ludox TMA silica, hybrids $\mathbf{C_1}$–$\mathbf{C_3}$, and silicas $\mathbf{D_1}$, $\mathbf{D_2}$

	Maximum particle diameter/μm					
Volume (%)	Ludox TMA[a]	$\mathbf{C_1}$	$\mathbf{C_2}$	$\mathbf{C_3}$	$\mathbf{D_1}$	$\mathbf{D_2}$
10.00	0.095	4.368	3.525	6.145	1.766	2.921
25.00	0.103	6.005	5.881	9.475	2.797	5.621
50.00	0.111	8.396	10.05	15.11	4.962	10.85
75.00	0.121	11.45	16.35	23.07	9.188	18.89
90.00	0.131	14.93	24.19	32.74	17.47	28.58

[a]Experimental data; manufacturer average particle diameter 22 nm.

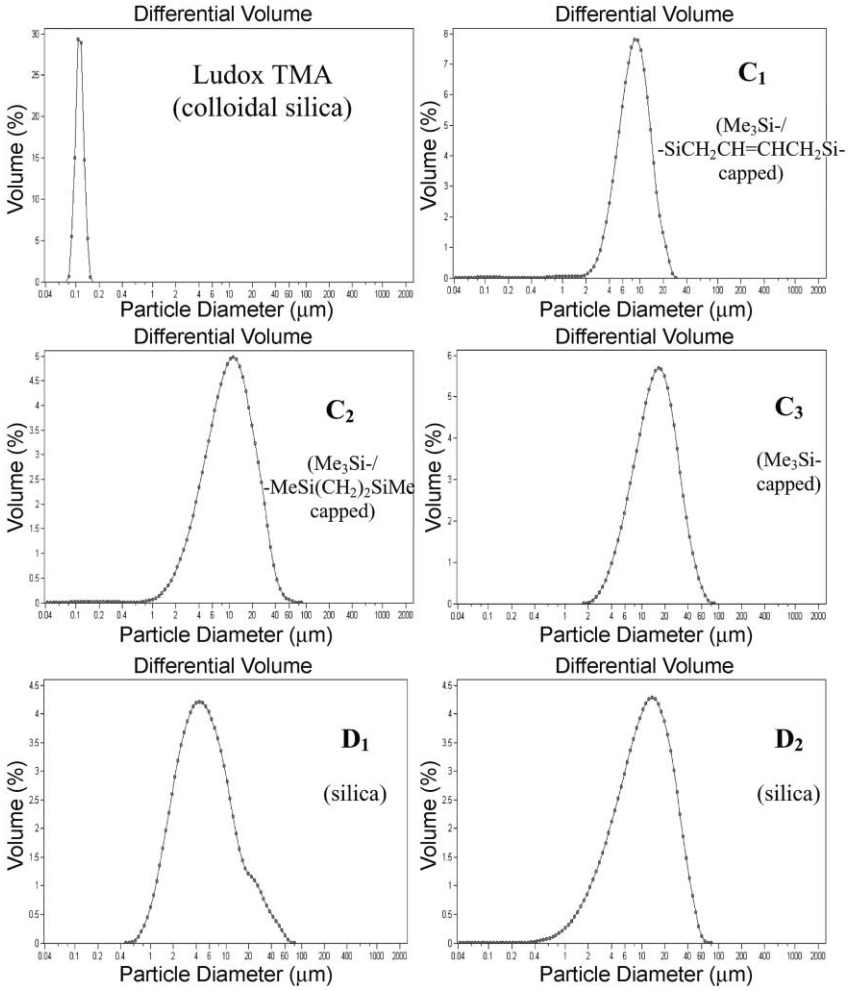

Fig. 3 Particle size distributions of Ludox TMA silica, hybrids $\mathbf{C_1}$–$\mathbf{C_3}$, and silicas $\mathbf{D_1}$, $\mathbf{D_2}$.

Table 4 N_2 BET surface area and porosity properties of hybrids $\mathbf{C_1}$–$\mathbf{C_3}$ and silicas $\mathbf{D_1}$, $\mathbf{D_2}$

Particle	Surface area/m^2 g^{-1}	Total pore volume/cm^3 g^{-1}	Micropore surface area/m^2 g^{-1}	Micropore volume/cm^3 g^{-1}	% Porosity
Ludox TMA	20[a]	/	/	/	/
$\mathbf{C_1}$	70	0.636	/	/	48.7
$\mathbf{C_2}$	99	0.556	/	/	45.4
$\mathbf{C_3}$	107	0.471	/	/	41.4
$\mathbf{D_1}$	131	0102	104	0.049	13.3
$\mathbf{D_2}$	399	0.356	364	0.225	34.9

[a]Estimated from experimental average particle diameter; manufacturer specific surface area 140 m^2 g^{-1}.

Particles $\mathbf{C_1}$, being smaller than particles $\mathbf{C_2}$ and $\mathbf{C_3}$ but also of narrower particle size distribution, were further studied. Oxidative treatment of $\mathbf{C_1}$, dispersed in methanol and THF, was performed using H_2O_2 (27.5 wt% in water) under nucleophilic catalysis (KF) or in slightly basic medium ($NaHCO_3$).[36] This led to particles $\mathbf{D_1}$ and $\mathbf{D_2}$, respectively (Scheme 2). Both particles were characterized by solid-state NMR spectroscopy. The ^{29}Si MAS NMR spectra exhibited only one similar set of signals for both $\mathbf{D_1}$ and $\mathbf{D_2}$, associated with Q ($Si(OSi)_4$) substructures from −90 to −120 ppm, confirming the oxidative degradation of the organic groups leading to silica particles. A major resonance was observed corresponding to Q^4 [$Si(OSi)_4$] and a minor Q^3 resonance [$Si(OH)(OSi)_3$ or $Si(OMe)(OSi)_3$], the particles $\mathbf{D_1}$ being slightly further condensed than $\mathbf{D_2}$ due to the nucleophilic catalysis of KF.

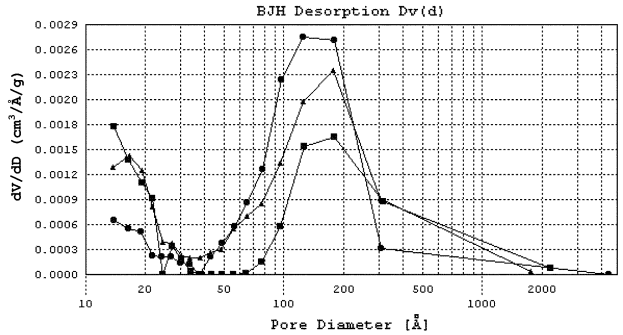

Fig. 4 Pore size distribution of hybrid particles $\mathbf{C_1}$–$\mathbf{C_3}$, calculated by the BJH method (■: $\mathbf{C_1}$; ▲: $\mathbf{C_2}$; ●: $\mathbf{C_3}$).

A much broader particle size distribution, however with a lower or similar average particle sizes of 5 and 11 μm, was observed for the silica particles $\mathbf{D_1}$ and $\mathbf{D_2}$, respectively, compared to the hybrid particle $\mathbf{C_1}$ (Table 3, Fig. 3). An important decrease of porosity and total pore volume was observed by N_2 sorption analysis: from 0.63 cm^3 g^{-1} for the hybrid $\mathbf{C_1}$, down to 0.36 and 0.10 cm^3 g^{-1}, $\mathbf{D_1}$ being less porous than $\mathbf{D_2}$ (Table 4). Moreover, the pore size distributions calculated by

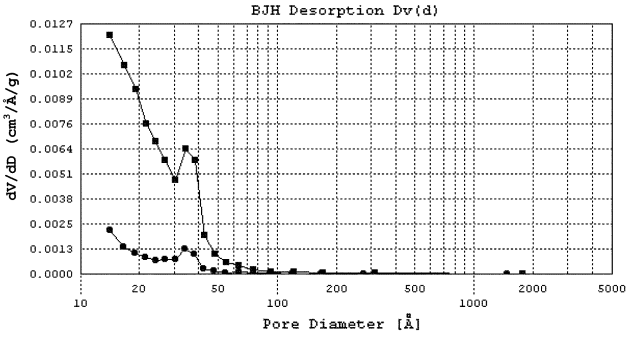

Fig. 5 Pore size distribution of hybrid particles $\mathbf{D_1}$ and $\mathbf{D_2}$, calculated by the BJH method (●: $\mathbf{D_1}$; ■: $\mathbf{D_2}$).

the BJH method for the particles $\mathbf{D_1}$ and $\mathbf{D_2}$ revealed the formation of largely microporous particles with some contribution in the mesoporous region, most of the pore diameters being however below 50 Å (Fig. 5). These results represented a major change compared to the BJH pore size distribution of the hybrid particles $\mathbf{C_1}$, which were, conversely, mostly above 50 Å, with some contribution in the micropore region.

The particle's size and porosity changes before and after chemical treatment revealed the important rearrangement of the silicate framework caused by the oxidative degradation of the organic groups. This was even more pronounced depending on the choice of reaction conditions used, a mild basic medium or a strong nucleophilic catalysis by fluoride ions, which probably further promoted structural rearrangements upon activation of the silicon atom.[37]

The second approach led to nanoporous silica particles of different porosity, 13 *versus* 35%, respectively for particles $\mathbf{D_1}$ and $\mathbf{D_2}$, but also of slightly different particle sizes and distribution, depending upon the reaction conditions used. The nanoporous silica particles $\mathbf{D_2}$ were of very similar surface area and total pore volume (up to 420 $m^2\ g^{-1}$ and 0.36 $cm^3\ g^{-1}$), to the silica particles $\mathbf{B_1}$ and $\mathbf{B_2}$ prepared by a different route. The particle size distribution of $\mathbf{D_2}$ was also very similar to particles $\mathbf{B_1}$ and $\mathbf{B_2}$; however the average particles size of the latter two were more than twice as small and below 5 μm.

Conclusion

We report here two simple routes for the preparation of stable porous silica particles. ORMOSIL particles were prepared in a first step either by a controlled sol–gel process or by co-condensation of colloidal silica nanoparticles with organosilicon precursors. Stable sub-micron hybrid particles of low porosity or mesoporous microparticles were then easily isolated. Removal of the templating organic spacer by different chemical treatments, eventually completed by calcination, led to carbon-free silica particles. High porosity and total pore volume, respectively up to 420 $m^2\ g^{-1}$ and 0.65 $cm^3\ g^{-1}$, and monomodal particle size distributions were demonstrated by both routes. These nanoporous silica particles of average particle size below 5 μm, being thermally stable up to 600 °C under air and dispersible in common organic solvents, are believed to offer interesting properties for a wider range of applications than conventional dense particles or porous gels.

Experimental

All reactions were carried out under nitrogen by use of a vacuum line and Schlenk tube techniques or three-neck flasks using anhydrous solvents. 1,4-Bis(trimethoxysilylethynyl)benzene, 1,4-bis(trimethoxysilyl)benzene, 1,4-bis(trichlorosilyl)but-2-ene were prepared as previously reported.[32] Chlorotrimethylsilane, 1,2-bis(dichloromethylsilyl)ethane and colloidal silica Ludox TMA were purchased from Aldrich. *N,O*-Bis(trimethylsilyl) carbamate (BSC) was purchased from Fluka.

Porosity measurements were carried out using the nitrogen sorption method on a Quantachrome Autosorb 1MP instrument. The surface areas were calculated using the BET equation, which is considered to give the total internal and external surface area of the material. The micropore surface areas and micropore volume were calculated using the de Boer *t*-method. Total pore volume is derived from the amount of vapour adsorbed at a relative pressure close to unity, by assuming that the pores are then filled with liquid adsorbate. Pore size distributions in the mesopore region are determined by the BJH. method. Samples were ultra-sonicated for several minutes prior to particle size determination on a Coulter LS 230 Laser Particles Size Analyser (from 0.04 to 2000 μm) using the Fraunhofer calculation model. Characterisation by spectroscopy was performed on a JEOL Lambda 400 MHz NMR instrument and a NICOLET 560 ESP FTIR.

Hybrid particles H_1

To 7.41 g (20.2 mmol) of 1,4-bis(trimethoxysilylethynyl)benzene and 67.4 mL of anhydrous THF was added 1.09 mL of distilled water at room temperature. The homogeneous solution was stirred for 2 days, prior to dropwise addition of 36.0 g of *N,O*-bis(trimethylsilyl) carbamate (BSC) in 100 mL of anhydrous dichloromethane. The reaction was exothermic and the solution became hazy with rapid formation of a soft gel. A faster addition of the BSC/CH_2Cl_2 mixture re-dispersed the solids into the solution. The mixture was heated at 30 °C for 5 h prior to addition of 11.2 g of methanol. A fast bubbling was observed significant of the reaction with an excess of capping agent. A further 20 mL of methanol were added at 30 °C. The mixture was then cooled down and the volatiles were evaporated under vacuum, leading to solid particles of visually different sizes, insoluble in any organic solvents. FTIR (KBr, ν/cm^{-1}): 1063, 1498, 2173, 2845, 2960, 3039 (weak), 3298. ^{13}C NMR (δ, ppm): 0.61, 49.1, 82.1 (weak), 88.8, 100.7, 122.1, 131.2. ^{29}Si CP MAS NMR (δ, ppm): 12.4, −78.1 (weak), −87.6, −97.3, −109.7 (weak). BET surface area: 37 $m^2\ g^{-1}$.

Hybrid particles H_2

To 7.26 g (19.8 mmol) of 1,4-bis(trimethoxysilylethynyl)benzene and 66.1 mL of anhydrous THF was added 1.07 mL of distilled water at room temperature. The homogeneous solution was stirred for 4 days when a further 200 mL of THF was added to reduce the viscosity. 32.8 g of *N,O*-bis(trimethylsilyl) carbamate (BSC) in 200 mL of THF were then added dropwise from −4 °C and slowly up to 13.7 °C. The milky solution was heated at 30 °C for 3 h and became clear. The mixture was cooled down to below 12 °C and 37 g of methanol were slowly added. The stable solution was left for 2 days at room temperature prior to evaporation under vacuum of the volatiles at 30 °C (5 mbar). The insoluble solid was kept in THF for particle size analysis. FTIR (KBr, ν/cm^{-1}): 1088, 1499, 2174, 2843, 2961, 3041 (very weak), 3303. ^{13}C NMR (δ, ppm): 1.4, 50.4, 82.8, 89.6, 101.2, 122.3, 131.8. ^{29}Si CP MAS NMR (δ, ppm): 11.5, −88.2, −97.9, −110.0 (very weak). BET surface area: 52 $m^2\ g^{-1}$.

Elimination of the organic fragment

The preparation of particles $\mathbf{A_1}$ and $\mathbf{B_1}$ is given as an example.

Hybrid particles A_1. To 5.07 g of hybrid particles $\mathbf{H_1}$ was added 80 mL of methanol, 80 mL of distilled water and 1 mL of a 1 M solution of NH_4F. The reactive medium was slightly refluxed at 70 to 75 °C under stirring for up to 3 days. The resulting solid was filtered on a Whatman paper 542 and washed several times with THF, and air-dried leading to an ivory powder $\mathbf{A_1}$. FTIR (KBr, ν/cm^{-1}): 1086, 1499, 2175, 2850, 2961, 3041, 3309. ^{29}Si MAS NMR (δ, ppm): 12.3, −98.66, −109.9. BET surface area: 257 $m^2\ g^{-1}$.

Silica particles B_1. Pyrolysis of hybrid particles A_1 (0.84 g) under an air flow at 600 °C for 4 h led to a white powder B_1 (0.60 g). FTIR (KBr, ν/cm^{-1}): 1097, 3442. ^{29}Si MAS NMR (δ, ppm): −100.0, −109.0. BET surface area: 416 m^2 g^{-1}.

Hybrid particles A_2. FTIR (KBr, ν/cm^{-1}): 1081, 2175, 2964. ^{29}Si MAS NMR (δ, ppm): 12.4, −100.8, −109.2. BET surface area: 402 m^2 g^{-1}.

Silica particles B_2. FTIR (KBr, ν/cm^{-1}): 1089, 3449. ^{29}Si MAS NMR (δ, ppm): −101.3, −109.8. BET surface area: 339 m^2 g^{-1}.

Preparation of hybrid particles C_1, C_2, C_3

The preparation of the hybrid particles C_1 is given as an example.

Hybrid particles C_1. 38.8 mL of concentrated HCl, 11.3 mL of distilled water, 50 ml of propan-2-ol, 66.4 g (614.8 mmol) of Me_3SiCl and 6.6 g (20.4 mmol) of 1,4-bis(trichlorosilyl)but-2-ene were mixed at low temperature in an ice/water bath until formation of a viscous solution occurred. A stream of this mixture was then added to 50 g of Ludox TMA colloidal silica in 200 mL of distilled water at room temperature. The solution was heated at 30 °C and a further 13.9 g (128.7 mmol) of Me_3SiCl were added. The hybrid silicate popped-out by further heating to 45 °C for 20 minutes. The aqueous phase was poured off, and distilled water was added several times to wash out the remaining HCl. The aqueous phase was poured off again, and 200 mL of toluene were added. The mixture was heated to reflux using a Dean–Stark trap to remove any remaining water. Solvent evaporation under vacuum led to 14.5 g of a white powder. FTIR (KBr, ν/cm^{-1}): 1110, 1615, 1638, 2846, 2958, 3017, 3370. ^{13}C MAS NMR (δ, ppm): 2.0, 16.0, 123.7. ^{29}Si MAS NMR (δ, ppm): 12.7, 8.4, −56.6, −66.0, −69.3, −102.7, −111.3. BET surface area: 70 m^2 g^{-1}.

Hybrid particles C_2. FTIR (KBr, ν/cm^{-1}): 1110, 1384, 2962, 3380. ^{29}Si CP MAS NMR (δ, ppm): 12.3, 8.3, −9.4, −18.8, −92.2, −101.4, −111.1. BET surface area: 99 m^2 g^{-1}.

Hybrid particles C_3. FTIR (KBr, ν/cm^{-1}): 1109, 2963, 3369. ^{29}Si MAS NMR (δ, ppm): 13.1, −102.2, −111.1. BET surface area: 107 m^2 g^{-1}.

Silica particles D_1. To 4.0 g of hybrid particles C_1 was added 78.6 mL of a 27.5 wt% solution of H_2O_2 in water, 100 mL of methanol, 100 mL of THF and 13.6 g of KF. The reactive medium was refluxed at 70 to 80 °C under stirring for up to 4 days. The resulting solid was purified by centrifugation, washed with distilled water and acetone, and air-dried leading to 4.0 g of a white powder D_1. ^{29}Si MAS NMR (δ, ppm): −98.9, −108.4, −168.6, 181.9. BET surface area: 131 m^2 g^{-1}.

Silica particles D_2. To 4.0 g of hybrid particles C_1 was added 78.6 mL of a 27.5 wt% solution of H_2O_2 in water, 100 mL of methanol, 100 mL of THF and 4.9 g of $NaHCO_3$. The reactive medium was refluxed at 70 to 80 °C under stirring for up to 4 days. The resulting solid was purified by centrifugation, washed with distilled water and acetone, and air-dried leading to 1.9 g of a white powder D_2. ^{29}Si MAS NMR (δ, ppm): −99.7, −108.7. BET surface area: 399 m^2 g^{-1}.

References

1 W. Stöber, A. Fink and E. Bohn, *J. Colloid Interface Sci.*, 1968, **26**, 62.
2 M. D. Sacks and T. Tseung-Yuen, *J. Am. Ceram. Soc.*, 1984, **67**, 526.
3 G. H. Bogush and C. F. Zukoski IV, in *Ultrastructure Processing of Advanced Ceramics*, ed J. D. Mackenzie and D. R. Ulrich, Wiley, New York, 1988, p. 477; G. H. Bogush and C. F. Zukoski IV, *J. Colloid Interface Sci.*, 1991, **142**, 1; G. H. Bogush and C. F. Zukoski IV, *J. Colloid Interface Sci.*, 1991, **142**, 19.
4 E. C. Ruvolo, H. L. Bellinetti and M. A. Aegerter, *J. Non-Cryst. Solids*, 1990, **121**, 244.
5 M. T. Harris, R. R. Brunson and C. H. Byers, *J. Non-Cryst. Solids*, 1990, **121**, 397.
6 T. Kawaguchi and K. Ono, *J. Non-Cryst. Solids*, 1990, **121**, 383.
7 R. Masuda, W. Takahasi and M. Ishii, *J. Non-Cryst. Solids*, 1990, **121**, 389.
8 H. Kozuka and S. Sakka, *Chem. Mater.*, 1989, **1**, 398; J. Yamaguchi, H. Kozuka and S. Sakka, *Trans. Mater. Res. Soc. Jpn.*, 1990, **1**, 140.
9 Q. Huo, J. Feng, F. Scuth and G. D. Stucky, *Chem. Mater.*, 1997, **9**, 14.
10 B. Kramkar, G. De, D. Kundu and D. Ganguli, *J. Non-Cryst. Solids*, 1991, **135**, 29; B. Karamkar, G. De and D. Ganguli, *J. Non-Cryst. Solids*, 2000, **272**, 119; G. De, B. Karmakar and D. Ganguli, *J. Mater. Chem.*, 2000, **10**, 2289.
11 J. Zaman and A. Chakma, *J. Membr. Sci.*, 1994, **92**, 1.
12 J. S. Beck, W. J. Vartuli, W. J. Roth, M. E. Leonowicz, C. T. Kresge, K. D. Schmitt, C. T. Chu, D. H. Olson, E. W. Sheppard and S. B. McCullen, *J. Am. Chem. Soc.*, 1992, **114**, 10834; C. T. Kresge, M. E. Leonowicz, W. J. Roth, J. C. Vartuli and J. S. Beck, *Nature*, 1992, **359**, 710.
13 P. Behrens, *Adv. Mater.*, 1993, **5**, 127.
14 M. E. Davis, *Nature*, 1993, **364**, 391.
15 M. Chai, Y. Yamasita, M. Machida, K. Eguchi and H. Arai, *J. Membr. Sci.*, 1994, **97**, 199; M. Chai, M. Machida, K. Eguchi and H. Arai, *J. Membr. Sci.*, 1994, **96**, 205.
16 A. Julbe, C. Guizard, A. Larbot, L. Cot and A. G. Fendler, *J. Membr. Sci.*, 1993, **77**, 137.
17 Y. Lu, L. Hang, C. J. Brinker, T. M. Niemczyk and G. P. Lopez, *Sens. Actuators, B*, 1996, **35**, 1; G. Cao, Y. Lu, G. P. Lopez and C. J. Brinker, *Adv. Mater.*, 1996, **8**, 588.
18 R. A. Peterson, M. A. Anderson and C. G. Hill Jr., *J. Membr. Sci.*, 1994, **94**, 103.
19 G. A. Ozin, *Chem. Commun.*, 2000, **8**, 723 and references therein.
20 M. Antonietti, B. Berton, C. Goltner and H. P. Hentze, *Adv. Mater.*, 1998, **10**, 154.
21 P. J. Bruinsma, A. Y. Kim, J. Liu and S. Baskaran, *Chem. Mater.*, 1997, **9**, 2507.
22 B. T. Holland, C. F. Blanford, T. Do and A. Stein, *Chem Mater.*, 1999, **11**, 795.
23 S. Schacht, Q. Huo, I. G. Voigt-Martin, G. D. Stucky and F. Schuth, *Science*, 1996, **273**, 768; D. Y. Zhao, P. D. Yang, B. F. Chmelka and G. D. Stucky, *Chem. Mater.*, 1999, **11**, 1174.
24 M. Grun and K. K. Unger, *Proc. Int. Zeolite Conf., 12th*, 1999, **2**, 757.
25 H. Fan, F. Van Swol, Y. Lu and C. J. Brinker, *J. Non-Cryst. Solids*, 2001, **285**, 71.
26 K. Imaizumi, T. Nakai, H. Shrasaka and K. Takeda, *Int. Conf. Process. Mater. Prop., 2nd*, 2000, 469.
27 S. H. Park and Y. N. Xia, *Chem. Mater.*, 1998, **10**, 1745.
28 O. D. Velev and E. W. Kaler, *Adv. Mater*, 1998, **12**, 531 and references therein.
29 H. Isobe and K. Kaneko, *J. Colloid Interface Sci.*, 1999, **212**, 234.
30 H. Mori and H. Yamashita, *J. Ceram. Soc. Jpn.*, 1993, **101**, 1180 and references therein.
31 A. Imhof and D. J. Pine, *Nature*, 1997, **389**, 948.
32 R. J. P. Corriu, J. J. E. Moreau, P. Thépot and M. Wong Chi Man, *Chem. Mater.*, 1992, **4**, 1217; P. M. Chevalier, R. J. P. Corriu, J. J. E. Moreau and M. Wong Chi Man, *J. Sol–Gel Sci. Technol.*, 1997, **8**, 603; P. Chevalier, R. J. P. Corriu, P. Delord, J. J. E. Moreau and M. Wong Chi Man, *New J. Chem.*, 1998, **22**, 5, 423; B. Boury, P. Chevalier, R. J. P. Corriu, P. Delord, J. J. E. Moreau and M. Wong Chi Man, *Chem. Mater.*, 1999, **11**, 2, 281.
33 S. Brunauer, P. H. Emmett and E. J. Teller, *J. Am. Chem. Soc.*, 1938, **60**, 309.
34 E. P. Barett, L. G. Joyner and P. H. Halenda, *J. Am. Chem. Soc.*, 1951, **73**, 373.
35 R. Evans, U. Marconi and P. Tarazona, *J. Chem. Soc., Faraday Trans. 2*, 1986, **82**, 1763.
36 K. Tamao, N. Ishida, T. Tanaka and M. Kumada, *Organometallics*, 1983, **2**, 1694.
37 R. J. P. Corriu and C. Guerin, *J. Organomet. Chem.*, 1980, **198**, 231; R. J. P. Corriu, C. Guerin and J. J. E. Moreau, *Top. Stereochem.*, 1985, **15**, 41 and references therein.